University of Groningen

A comparison of a statistical-mechanics based plasticity model with discrete dislocation plasticity calculations

Yefimov, S; Groma, [No Value]; van der Giessen, Erik; Groma, I.

IMPORTANT NOTE: You are advised to consult the publisher's version (publisher's PDF) if you wish to cite from it. Please check the document version below.

Document Version
Publisher's PDF, also known as Version of record

Publication date:
2004

Link to publication in University of Groningen/UMCG research database

A comparison of a statistical-mechanics based plasticity model with discrete dislocation plasticity calculations

S. Yefimov[a], I. Groma[b], E. van der Giessen[a],*

[a] *Department of Applied Physics, University of Groningen, Nyenborgh 4, 9747 AG Groningen, The Netherlands*
[b] *Eötvös University, Dept. of General Physics, Pazmany P. setany 1/b, Pf. 32 H-1518 Budapest, Hungary*

Abstract

A two-dimensional nonlocal version of continuum crystal plasticity theory is proposed, which is based on a statistical-mechanics description of the collective behavior of dislocations coupled to standard small-strain crystal continuum kinematics for single slip. It involves a set of transport equations for the total dislocation density field and for the net-Burgers vector density field, which include a slip system back stress associated to the gradient of the net-Burgers vector density. The theory is applied to the problem of shearing of a two-dimensional composite material with elastic reinforcements in a crystalline matrix. The results are compared to those of discrete dislocation simulations of the same problem. The continuum theory is shown to be able to pick up the distinct dependence on the size of the reinforcing particles for one of the morphologies being studied. Also, its predictions are consistent with the discrete dislocation results during unloading, showing a pronounced Bauschinger effect. None of these features are captured by standard local plasticity theories.
© 2003 Elsevier Ltd. All rights reserved.

Keywords: A. Dislocations; B. Constitutive behavior; B. Crystal plasticity; B. Metallic materials; C. Finite elements

1. Introduction

Crystal plasticity theories have become popular and successful models for the anisotropic plastic deformation of single crystals. They have a hybrid, discrete/continuum,

---

* Corresponding author. Tel.: +31-50-363-8047; fax: +31-50-363-4881.
 E-mail address: giessen@phys.rug.nl (E. van der Giessen).

nature in the sense that they adopt a continuum description of the plastic flow by averaging over dislocations, but account for the discreteness of the available slip systems. Constitutive descriptions of the flow strengths and the hardening matrix have been given on purely phenomenological grounds, by e.g. Asaro (1983), but also on the basis of dislocation models, e.g. by Kocks et al. (1975).

Irrespective of the precise formulation, conventional continuum plasticity theory predicts that the plastic response is size independent. There is a considerable, and growing, body of experimental evidence, however, that shows that the response is in fact size dependent at length scales of the order of tens of microns and smaller, e.g. Fleck et al. (1994), Ma and Clarke (1995) and Stölken and Evans (1998). Various so-called nonlocal plasticity theories have been proposed that incorporate a size dependence, e.g. Aifantis (1984), Fleck and Hutchinson (1997), Acharya and Bassani (2000), Gurtin (2000, 2002), but they differ strongly in origin and mathematical structure. Although dislocation-based arguments have sometimes been used as a motivation, the theories mentioned above are phenomenological and have not been quantitatively derived from considerations of the behavior of dislocations. Therefore, the material length scale that enters in such theories needs to be fitted to experimental results (see, e.g., Fleck et al., 1994; Fleck and Hutchinson, 1997) or results of numerical discrete dislocation simulations, e.g. Bassani et al. (2001), Bittencourt et al. (2003).

This paper is concerned with a new nonlocal plasticity theory that combines a standard crystal plasticity model with a two-dimensional statistical-mechanics description of the collective behavior of dislocations due to Groma (1997) and to Groma and Balogh (1999). The resulting theory contains a length scale through a set of coupled transport equations for two dislocation density fields: one is the total dislocation density and the other is a net-Burgers vector density. After a summary of the theory for single slip, we proceed to numerical implementation of the theory and to a comparison with direct simulations of discrete dislocation plasticity in a model composite material based on the work of Cleveringa et al. (1997, 1998, 1999a). Similar comparisons have been carried out by Bassani et al. (2001) and Bittencourt et al. (2003) with the nonlocal theories of Acharya and Bassani (2000) and Gurtin (2002), respectively.

2. Statistical-mechanics description for single slip

Let us consider N parallel edge dislocations positioned at the points r^i, $i = 1, \ldots, N$, in $\mathbb{R}^2$. In single slip, the Burgers vector of the ith dislocation is $b^i = \pm b$ where b is parallel to the slip direction s, i.e. $b = bs$. With the commonly accepted assumption of over-damped dislocation motion, the glide velocity of the ith dislocation in the slip direction s is given by $v^i = B^{-1}F^i$ in terms of the dislocation drag coefficient B and the glide component of the Peach-Koehler force, F^i. This can be further elaborated as

$$v^i = B^{-1}b^i \left(\sum_{j \neq i}^{N} \tau_{\text{ind}}(r^i - r^j) + \tau_{\text{ext}}(r^i) \right), \tag{1}$$

where τ_{ind} is the shear stress at position $\boldsymbol{r}^i$ created by the dislocation at $\boldsymbol{r}^j$ and τ_{ext} is the external resolved shear stress field.

The passage to a continuum description is carried out with a special averaging procedure explained in detail in (Groma, 1997; Groma and Balogh, 1999). By coarse-graining the discrete dislocation distribution into densities of dislocations with positive or negative signs—ρ_+ and ρ_-, respectively—one can arrive at the following balance equations:

$$\dot{\rho}_+(\boldsymbol{r},t) + B^{-1}\frac{\partial}{\partial \boldsymbol{r}} \cdot \boldsymbol{b}\left[\int\{\rho_{++}(\boldsymbol{r},\boldsymbol{r}',t) - \rho_{+-}(\boldsymbol{r},\boldsymbol{r}',t)\}\right.$$

$$\left. \times \tau_{\mathrm{ind}}(\boldsymbol{r}-\boldsymbol{r}',t)\mathrm{d}^2\boldsymbol{r}' + \rho_+(\boldsymbol{r},t)\tau_{\mathrm{ext}}(\boldsymbol{r},t) \right] = 0, \tag{2}$$

$$\dot{\rho}_-(\boldsymbol{r},t) + B^{-1}\frac{\partial}{\partial \boldsymbol{r}} \cdot \boldsymbol{b}\left[\int\{\rho_{--}(\boldsymbol{r},\boldsymbol{r}',t) - \rho_{-+}(\boldsymbol{r},\boldsymbol{r}',t)\}\right.$$

$$\left. \times \tau_{\mathrm{ind}}(\boldsymbol{r}-\boldsymbol{r}',t)\mathrm{d}^2\boldsymbol{r}' - \rho_-(\boldsymbol{r},t)\tau_{\mathrm{ext}}(\boldsymbol{r},t) \right] = 0, \tag{3}$$

where $(\ )\cdot(\ )$ is the usual scalar product of two vectors, a superposed dot denotes the time (t) derivative and where $\rho_{++}, \rho_{+-}, \rho_{-+}, \rho_{--}$ are the two-particle density functions with the corresponding signs. For the further considerations it is useful to introduce the total dislocation density, ρ, and the sign density, κ, by

$$\rho(\boldsymbol{r},t) = \rho_+(\boldsymbol{r},t) + \rho_-(\boldsymbol{r},t), \quad \kappa(\boldsymbol{r},t) = \rho_+(\boldsymbol{r},t) - \rho_-(\boldsymbol{r},t).$$

The latter is a measure of the density of net-Burgers vector, and therefore is equivalent to the density of geometrically necessary dislocations (GNDs). By adding and subtracting Eqs. (2)–(3) we arrive at

$$\dot{\rho}(\boldsymbol{r},t) + B^{-1}\frac{\partial}{\partial \boldsymbol{r}} \cdot \boldsymbol{b}\left[\int \kappa^{(2)}(\boldsymbol{r},\boldsymbol{r}',t)\tau_{\mathrm{ind}}(\boldsymbol{r}-\boldsymbol{r}',t)\mathrm{d}^2\boldsymbol{r}' + \kappa(\boldsymbol{r},t)\tau_{\mathrm{ext}}(\boldsymbol{r},t) \right] = 0, \tag{4}$$

$$\dot{\kappa}(\boldsymbol{r},t) + B^{-1}\frac{\partial}{\partial \boldsymbol{r}} \cdot \boldsymbol{b}\left[\int \rho^{(2)}(\boldsymbol{r},\boldsymbol{r}',t)\tau_{\mathrm{ind}}(\boldsymbol{r}-\boldsymbol{r}',t)\mathrm{d}^2\boldsymbol{r}' + \rho(\boldsymbol{r},t)\tau_{\mathrm{ext}}(\boldsymbol{r},t) \right] = 0 \tag{5}$$

with

$$\kappa^{(2)}(\boldsymbol{r},\boldsymbol{r}',t) = \rho_{++}(\boldsymbol{r},\boldsymbol{r}',t) + \rho_{--}(\boldsymbol{r},\boldsymbol{r}',t) - \rho_{+-}(\boldsymbol{r},\boldsymbol{r}',t) - \rho_{-+}(\boldsymbol{r},\boldsymbol{r}',t),$$

$$\rho^{(2)}(\boldsymbol{r},\boldsymbol{r}',t) = \rho_{++}(\boldsymbol{r},\boldsymbol{r}',t) - \rho_{--}(\boldsymbol{r},\boldsymbol{r}',t) - \rho_{+-}(\boldsymbol{r},\boldsymbol{r}',t) + \rho_{-+}(\boldsymbol{r},\boldsymbol{r}',t).$$

It is important to note that Eqs. (4) and (5) are exact, i.e. they are obtained from (1) without any assumptions. However, since they depend on the two-particle distribution functions they do not form a closed set of equations. Although equations can be derived for the two-particle densities, they depend on the three-particle densities (Groma, 1997) etc., resulting in a hierarchy of equations. In order to arrive at a set of evolution equations in closed form, this chain of equations has to be cut by assuming a form for a certain order correlation function.

Numerical investigations by Zaiser et al. (2001) and Groma et al. (2003) have revealed that the dislocation–dislocation correlations in a homogeneous system have a short-range character. Therefore, it is plausible to assume that for a system not far from being homogeneous, the two-particle density functions $\rho_{ij}(\mathbf{r}, \mathbf{r}', t)$ can be given in the form

$$\rho_{ij}(\mathbf{r}, \mathbf{r}', t) = \rho_i(\mathbf{r})\rho_j(\mathbf{r}')[1 + d_{ij}(\mathbf{r}, \mathbf{r}')] \quad i, j = +, -, \tag{6}$$

where d_{ij} corresponds to the correlation function of a homogeneous dislocation system. As a consequence, d_{ij} depends only on the relative coordinate $\mathbf{r} - \mathbf{r}'$. The actual form of d_{ij} can be determined either from discrete numerical simulations or from an equation obtained by cutting the hierarchy of the above-mentioned equations at second order; for details, see (Zaiser et al., 2001).

Note that nucleation and annihilation of dislocations are not considered in (4) and (5) at this stage since the analysis is for a fixed number of dislocations. The nucleation and annihilation of dislocations can be taken into account by adding a source term to the right-hand side of Eq. (4). However, Eq. (5) has to remain unchanged reflecting that for the coarse-graining area (with sizes of a few dislocation distances) introduced for the derivation of Eqs. (2) and (3), dislocation multiplication or annihilation cannot modify the net-Burgers vector, i.e. the number of GNDs is "locally" conserved.

With the above assumption and taking (6) into account, we can rewrite the evolution equations (4) and (5) in the form

$$\dot{\rho} + B^{-1}\frac{\partial}{\partial \mathbf{r}} \cdot \mathbf{b}\kappa\{\tau_{\text{int}} + \tau_{\text{ext}} - \tau_{\text{s}}\} = f(\rho, \kappa, \ldots), \tag{7}$$

$$\dot{\kappa} + B^{-1}\frac{\partial}{\partial \mathbf{r}} \cdot \mathbf{b}\rho\{\tau_{\text{int}} + \tau_{\text{ext}} - \tau_{\text{s}}\} = 0, \tag{8}$$

in which $f(\rho, \kappa, \ldots)$ is a term describing the dislocation creation and annihilation (to be specified later),

$$\tau_{\text{int}}(\mathbf{r}) = \int \kappa(\mathbf{r}')\tau_{\text{ind}}(\mathbf{r} - \mathbf{r}') \, \mathrm{d}^2\mathbf{r}' \tag{9}$$

is the self-consistent, internal stress field created by the dislocations, and

$$\tau_{\text{s}}(\mathbf{r}) = -\int \kappa(\mathbf{r}')d^t(\mathbf{r} - \mathbf{r}')\tau_{\text{ind}}(\mathbf{r} - \mathbf{r}') \, \mathrm{d}^2\mathbf{r}' \tag{10}$$

is due to dislocation–dislocation correlations and will be referred to as back stress. Here we have introduced $d^t(\mathbf{r}) = [2d_{++}(\mathbf{r}) + d_{+-}(\mathbf{r}) + d_{+-}(-\mathbf{r})]/4$, taking into account that in a homogeneous system $d_{++}(\mathbf{r}) = d_{--}(\mathbf{r})$ and $d_{+-}(\mathbf{r}) = d_{-+}(-\mathbf{r})$.

Since the function $d^t(\mathbf{r})$ decays to zero within a few dislocation distances (for details, see Zaiser et al., 2001), the Taylor expansion of $\kappa(\mathbf{r}')$ around the point $\mathbf{r}$ can be used to approximate the integral in (10) by the form (keeping only the first non-vanishing term)

$$\tau_{\text{s}}(\mathbf{r}) = \frac{\partial \kappa}{\partial \mathbf{r}} \cdot \int (\mathbf{r} - \mathbf{r}')d^t(\mathbf{r} - \mathbf{r}')\tau_{\text{ind}}(\mathbf{r} - \mathbf{r}') \, \mathrm{d}^2\mathbf{r}'. \tag{11}$$

Next, we note that $d^t(\mathbf{r})$ does not depend directly on $\mathbf{r}$ but through $\sqrt{\rho}\mathbf{r}$, because of dimensional considerations. Furthermore, since the shear stress $\tau_{\text{ind}}(\mathbf{r})$ is proportional to $1/r$, the expression (11) can be rewritten as

$$\tau_s(\mathbf{r}) = \frac{\partial \kappa}{\partial \mathbf{r}} \cdot \frac{1}{\rho(\mathbf{r})} \int \mathbf{x}\, d^t(\mathbf{x})\tau_{\text{ind}}(\mathbf{x})\,\mathrm{d}^2\mathbf{x} \quad \text{with } \mathbf{x} = \sqrt{\rho}\mathbf{r}. \tag{12}$$

From the actual, well-known (Hirth and Lothe, 1968) shear stress field of a single dislocation, $\tau_{\text{ind}}(\mathbf{r})$, one can finally conclude that

$$\tau_s(\mathbf{r}) = \frac{\mu \mathbf{b}}{2\pi(1-v)\rho(\mathbf{r})} \cdot D\, \frac{\partial \kappa}{\partial \mathbf{r}} \tag{13}$$

where μ is the shear modulus, v is Poisson's ratio, and D is a dimensionless constant.

It should be mentioned that Groma et al. (2003) have put forward a more elaborate version of the theory, which leads to an additional stress contribution. Here we confine attention to the previous version of Groma (1997) and Groma and Balogh (1999).

3. Incorporation into crystal plasticity theory

The above description of the dislocation structure in terms of the density fields ρ and κ is incorporated into the well-known framework of single crystal continuum plasticity (see, e.g., Asaro, 1983). Confining attention to small displacement gradients, the total strain rate $\dot{\boldsymbol{\varepsilon}}$ in such a constitutive model is decomposed as

$$\dot{\boldsymbol{\varepsilon}} = \dot{\boldsymbol{\varepsilon}}^e + \dot{\boldsymbol{\varepsilon}}^p \tag{14}$$

in terms of the elastic strain rate $\dot{\boldsymbol{\varepsilon}}^e$ and the plastic strain rate $\dot{\boldsymbol{\varepsilon}}^p$ which, for single slip, is expressed in terms of the slip rate $\dot{\gamma}$ on the slip system as

$$\dot{\boldsymbol{\varepsilon}}^p = \tfrac{1}{2}\dot{\gamma}(\mathbf{s} \otimes \mathbf{m} + \mathbf{m} \otimes \mathbf{s}). \tag{15}$$

Here, $\mathbf{m}$ is the unit normal vector on the slip planes and $\mathbf{s}$ is the slip direction; in this case $\mathbf{s} = \mathbf{b}/|\mathbf{b}|$. The elastic strain rate is governed by Hooke's law in the form

$$\dot{\boldsymbol{\varepsilon}}^e = \mathscr{L}^{-1}\dot{\boldsymbol{\sigma}}, \tag{16}$$

with $\dot{\boldsymbol{\sigma}}$ the stress rate and $\mathscr{L}$ the tensor of elastic moduli, which is expressed in terms of μ and v for isotropic elasticity.

The coupling between crystal plasticity and dislocation densities comprises two steps:

1. The driving stress $\tau_{\text{int}} + \tau_{\text{ext}}$ appearing in the evolution equations (7)–(8) is approximated by the resolved shear stress based on the continuum stress field $\boldsymbol{\sigma}$, i.e.

$$\tau_{\text{int}} + \tau_{\text{ext}} \equiv \tau = \mathbf{m} \cdot \boldsymbol{\sigma} \cdot \mathbf{s}. \tag{17}$$

Note that this shear stress is a local quantity, i.e. determined only by quantities at the continuum point $\mathbf{r}$. τ_{ext} is the local stress in the dislocated body applied through the boundary conditions, τ_{int} is the local internal stress due to the collective fields of all dislocations irrespective of any dislocation–dislocation correlation. Correlation

between dislocations is taken into account in a first approximation by the back stress τ_s. This is determined by the gradient of the κ field, see Eq. (13), and therefore is nonlocal in nature.

2. The slip rate $\dot{\gamma}$ is related to the dislocation density and to the average (in the usual continuum sense) dislocation velocity $\boldsymbol{v}$ through Orowan's relation [1] $\dot{\gamma} = \rho \boldsymbol{b} \cdot \boldsymbol{v}$. With $\boldsymbol{v}$ being approximated by

$$\boldsymbol{v} = B^{-1}\boldsymbol{b}(\tau - \tau_s), \tag{18}$$

similar to (1), we obtain

$$\dot{\gamma} = B^{-1}b^2\rho(\tau - \tau_s). \tag{19}$$

In addition, we stipulate that the response of the material be elastic, i.e. $\dot{\gamma} = 0$, when

$$|\tau - \tau_s| < \tau_{res}, \tag{20}$$

where τ_{res} is the slip resistance. This quantity can take into account the effect of obstacles on the slip plane in the form of small precipitates or forest dislocations.

This results in a closed system of equations once the source term in Eq. (7) is specified. At this point, various propositions have been made, e.g. Groma (1997) and Groma and Balogh (1999). Let us first look at the nucleation and annihilation mechanism incorporated in the discrete dislocation simulations of Cleveringa et al. (1997, 1998, 1999a) which will serve as "numerical experiments" for verification in a subsequent section.

In these simulations, based on the discrete dislocation plasticity description proposed by Van der Giessen and Needleman (1995), new dislocations are generated by mimicking the Frank-Read mechanism. In two dimensions, a Frank-Read source is emulated by a point source on the slip plane which generates a dislocation dipole when the magnitude of the resolved shear stress at the source exceeds the source strength τ_{nuc} during a period of time t_{nuc}. Annihilation of two dislocations on the same slip plane with opposite Burgers vectors occurs when they are within a material-dependent, critical annihilation distance L_e, which is taken to be $L_e = 6b$ (Cleveringa et al., 1997, 1998, 1999a). As we are here aiming at a comparison with the discrete dislocation results in these references, we choose a form of the source term in (7) that mimics the above-mentioned nucleation and annihilation rules:

$$f(\rho, \kappa, \ldots) = C\rho_{nuc}|\tau - \tau_s| - AL_e(\rho + \kappa)(\rho - \kappa)|v|. \tag{21}$$

The first term in the right-hand side represents nucleation from sources with a density ρ_{nuc} and at a rate governed by the parameter C given by

$$C = \frac{1}{\tau_{nuc}t_{nuc}} \text{ if } |\tau - \tau_s| \geqslant \tau_{nuc}, \quad C = 0 \text{ otherwise}, \tag{22}$$

in terms of the nucleation strength τ_{nuc} and the nucleation time t_{nuc}. The second term in the right-hand side of (21) describes the annihilation of positive and negative dislocations, with densities $\rho_+ = \frac{1}{2}(\rho + \kappa)$ and $\rho_- = \frac{1}{2}(\rho - \kappa)$ respectively, at a rate determined

---

[1] We do not include a term with $\dot{\rho}$ in $\dot{\gamma}$ for freshly generated dislocations since they have not glided yet and therefore have not produced slip.

by $A|v|$, with A is a dimensionless constant. This is similar in spirit to the proposition by Tabourot et al. (2001) that the annihilation rate is proportional to $\rho\dot{\gamma}b^{-1} = \rho^2 v$. However, since we distinguish here between positive and negative dislocations, the annihilation term in (21) with ρ^2 replaced by $\rho_+\rho_-$ more closely reflects the annihilation mechanism.

It is of importance to note that the set of Eqs. (7)–(8) and (14)–(21) is a particular non-local theory. The material length scale is introduced in the evolution equations (7)–(8) via the gradient terms. These equations are similar in form to the reaction–diffusion-based model proposed by Aifantis (1984), but in the present model they are actually derived from a statistical-mechanics description of dislocation glide. Even though they have the mathematical structure of diffusion equations, they physically represent conservations laws for dislocation densities during dislocation glide.

4. Application to a metal–matrix composite

4.1. Problem formulation

As a first application of the theory we consider the deformation of a two-dimensional model material containing rectangular particles arranged in a doubly periodic hexagonal packing, as illustrated in Fig. 1. This is the same problem as analyzed using discrete dislocation dynamics by Cleveringa et al. (1997, 1998, 1999a), and is used to check the quality of the present nonlocal theory in reproducing the size-dependent results. Two reinforcement morphologies are analyzed which have the same area fraction of 20% but different geometric arrangements of the reinforcing phase. In one morphology, called
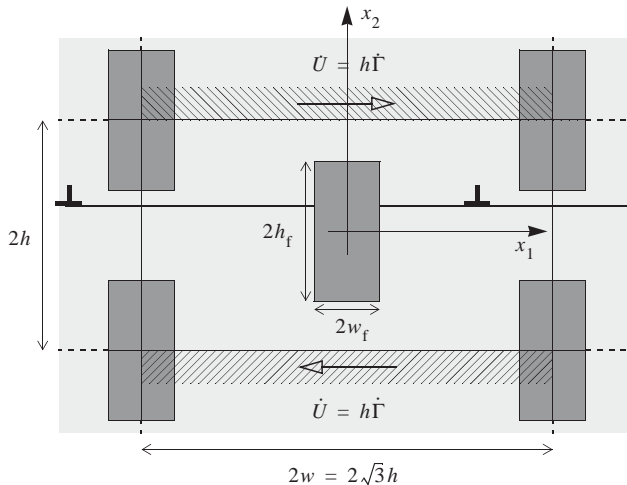

Fig. 1. Simple shear of a model composite material with elastic reinforcements in a hexagonal pattern. All slip planes are parallel to the shearing direction x_1.

material (i) by Cleveringa et al. (1997), the particles are square and are separated by unreinforced veins of matrix material while in the other, referred to as material (iii), the particles are rectangular and do not leave any unreinforced veins of matrix material.

Because of periodicity, a unit cell analysis is carried out with each cell having width $2w$ and height $2h$ ($w/h = \sqrt{3}$), see Fig. 1. The particles are of size $2w_f \times 2h_f$ with $h_f = w_f = 0.416h$ for material (i) and $h_f = 2w_f = 0.588h$ for material (iii). The half-height of the unit cell, h, is expressed in terms of the material length scale L which in turn is taken to be $L = 4000b$. The effect of particle size is studied by varying h/L (recall that L is just a fixed reference length).

The reinforcing particles remain elastic with shear modulus $\mu^* = 192.3$ GPa and Poisson ratio $v^* = 0.17$. The matrix material also has isotropic elastic properties, but with $\mu = 26.3$ GPa and $v = 0.33$. These values are representative for silicon carbide particles in an aluminum matrix. The matrix material can undergo plastic deformation by single slip with the slip plane normal $\boldsymbol{m}$ being in the x_2-direction and the Burgers vector $\boldsymbol{b}$ parallel to the x_1-direction, see Fig. 1. The magnitude of the Burgers vector is $b = 0.25$ nm and the drag coefficient is $B = 10^{-4}$ Pa s.

The unit cell is subjected to plane-strain simple shear, which is prescribed through the macroscopic boundary conditions

$$u_1(t) = \pm h\Gamma(t), \quad u_2(t) = 0 \text{ along } x_2 = \pm h, \tag{23}$$

where $\Gamma(t)$ is the applied macroscopic shear at time t. Periodic boundary conditions are imposed along the lateral sides $x_1 = \pm w$. The overall shear stress $\bar{\tau}$ needed to sustain this deformation is calculated from the virtual work statement

$$\int_V \boldsymbol{\sigma} : \boldsymbol{\varepsilon} \, \mathrm{d}V = \int_S \boldsymbol{T}_0 \cdot \boldsymbol{u} \, \mathrm{d}S, \tag{24}$$

by using the actual displacement ($\boldsymbol{u}$) and associated strain field ($\boldsymbol{\varepsilon}$) as virtual fields. The vector $\boldsymbol{T}_0$ is the traction on the boundary S of the region V. The boundary integral consists of contributions of the boundary $S_1 = \{x_1 = \pm w\} \subset S$, which cancel because of periodicity, and of two contributions from the boundary $S_2 = \{x_2 = \pm h\} = S \setminus S_1$, which add up to $2(\bar{\tau}h\Gamma 2w)$. Hence, the overall shear stress $\bar{\tau}$ is calculated from

$$\bar{\tau} = \frac{1}{4wh\Gamma} \int_{-w}^{w} \int_{-h}^{h} \boldsymbol{\sigma} : \boldsymbol{\varepsilon} \, \mathrm{d}x_1 \, \mathrm{d}x_2. \tag{25}$$

A constant macroscopic strain rate, $\dot{\Gamma}$, is imposed until a specified shear strain Γ is reached. Then, the material is unloaded by applying $\dot{\Gamma}$ in the opposite direction until the average shear stress $\bar{\tau}$ vanishes.

In addition to these purely mechanical boundary conditions, we specify conditions on dislocation motion along the interfaces with the elastic particles, by requiring these interfaces to be impenetrable.

4.2. Numerical implementation of the continuum model

We begin by expressing the evolution equations (7)–(8) in the particular form for the present problem, where $\boldsymbol{b} = b\boldsymbol{e}_1$ everywhere in the matrix (with $\boldsymbol{e}_i$ being the Cartesion

base vectors associated with the coordinates x_i), see Fig. 1. Hence,

$$\dot{\rho} + B^{-1} \frac{\partial}{\partial x_1} [b\kappa(\tau - \tau_s)] = f(\rho, \kappa, \ldots), \tag{26}$$

$$\dot{\kappa} + B^{-1} \frac{\partial}{\partial x_1} [b\rho(\tau - \tau_s)] = 0. \tag{27}$$

Making reference to the expression (18) for the continuum dislocation velocity v, we see that the evolution law for the κ field is determined by the gradient of ρv in the slip direction. This observation helps us in formulating physically meaningful boundary conditions along the cell boundaries S as well as along the particle boundaries S^p. First of all, along the cell sides $S_1 = \{x_1 = \pm w\}$ with unit outer normal vector $\boldsymbol{n} = \pm \boldsymbol{e}_1$, periodic boundary conditions are applied, so that $\rho(w, x_2) = \rho(-w, x_2)$ and $\kappa(w, x_2) = \kappa(-w, x_2)$ at all times. Along $S_2 = \{x_2 = \pm h\}$ with $\boldsymbol{n} = \pm \boldsymbol{e}_2$ we have the natural boundary condition that there is no flux of dislocations across these boundaries since the slip plane is parallel to these boundaries. The conditions along the matrix–particle interfaces, S^p, fall apart in two groups. First, there is a similar natural boundary condition of no dislocation flux across interfaces with the normal in the x_2-direction, $S_2^p \subset S^p$. Second, on the ones with normals in the x_1-direction, $S_1^p = S^p \setminus S_2^p$, we require the dislocation flux to vanish, i.e. $v_1 = 0$, because the particles are impenetrable. In summary, we can write

$$\kappa v_1 n_1 = \rho v_1 n_1 = 0 \quad \text{on matrix boundaries } S_2 \cup S^p \tag{28}$$

with n_1 the component of boundary normal $\boldsymbol{n}$ in the slip direction.

The dislocation density evolution equations (26)–(27) supplemented with the boundary conditions (28) represent a non-linear convection-dominated diffusion problem coupled to the single crystal continuum plasticity model described in Section 3. A straightforward finite element method is employed here to solve this set of equations.

The dislocation evolution part of the problem and the crystal plasticity part can be decoupled by applying a staggered solution procedure for time integration. The solution of either of the two separate problems is obtained by using an explicit time-stepping scheme, with the same time steps for both subproblems. In principle, we may adopt independent spatial discretizations for the two parts of the problem, but we take the two meshes to be identical for convenient passing of information. The spatial discretization is based on quadrilateral elements consisting of four crossed linear triangular elements.

As we are limiting attention to small strains, the solution of the crystal plasticity part departs directly from the incremental version of the principle of virtual work (24). The associated boundary conditions have already been listed in (23).

In addition, we solve the evolution equations (26)–(27) in the matrix using a standard weighted-residual Galerkin method. It is well-known that this is generally not an adequate method for convection-dominated problems. However, since the objective here is not to present an effective numerical method but to demonstrate the predictions of the constitutive theory, the priority at this stage is not the implementation of more complicated upwinding methods, see e.g. Morton (1996). Therefore, we adopt a straightforward Galerkin method, and choose mesh and time stepping so as to retain the necessary accuracy for the desired proof of principle. The spatial discretization is

based on the interpolation of ρ and κ, as well as their rates, inside an element from the nodal values; e.g.

$$\rho = \mathbf{N}^{\mathrm{T}}\boldsymbol{\rho}, \tag{29}$$

$$\kappa = \mathbf{N}^{\mathrm{T}}\boldsymbol{\kappa}, \tag{30}$$

where $\boldsymbol{\rho}$ and $\boldsymbol{\kappa}$ are the vectors of nodal values of the dislocation densities ρ and κ, respectively, and $\mathbf{N}$ is the vector of the C_0 continuous shape functions. As a consequence, the back stress according to (13), i.e.

$$\tau_{\mathrm{s}} = b\frac{T}{\rho}\frac{\partial\kappa}{\partial x_1}, \quad T = D\frac{\mu}{2\pi(1-v)} \tag{31}$$

is governed by lower-dimensional interpolation. Therefore, we take the back stresses to be defined at the integration points of elements, just like the resolved shear stress from (17).

After substitution of (31) and evaluation of the weighted residual integral for the balance law (27) for κ, for instance, we obtain the system of linear equations

$$\mathbf{M}\dot{\boldsymbol{\kappa}} = \mathbf{J}\boldsymbol{\rho} - \mathbf{H}\boldsymbol{\kappa} - \mathbf{f}. \tag{32}$$

Here,

$$\mathbf{M} = \int_{-w}^{w}\int_{-h}^{h}\mathbf{N}\mathbf{N}^{\mathrm{T}}\,\mathrm{d}x_1\,\mathrm{d}x_2 \tag{33}$$

is the standard mass matrix;

$$\mathbf{J} = B^{-1}b\int_{-w}^{w}\int_{-h}^{h}\tau\mathbf{N}\frac{\partial\mathbf{N}^{\mathrm{T}}}{\partial x_1}\,\mathrm{d}x_1\,\mathrm{d}x_2 \tag{34}$$

is the nonsymmetric matrix of the convective term; and

$$\mathbf{H} = B^{-1}b^2\int_{-w}^{w}\int_{-h}^{h}T\frac{\partial\mathbf{N}}{\partial x}\frac{\partial\mathbf{N}^{\mathrm{T}}}{\partial x}\,\mathrm{d}x_1\,\mathrm{d}x_2 \tag{35}$$

is the diffusion matrix. Note that in the derivation of this term, the density ρ in the numerator of the convective term of (27) cancels the ρ in the denominator of (31). The right-hand side vector

$$\mathbf{f} = \int_{S_1}\mathbf{N}^{\mathrm{T}}\rho v_1 n_1\,\mathrm{d}S + \int_{S_2\cup S^{\mathrm{p}}}\mathbf{N}^{\mathrm{T}}\rho v_1 n_1\,\mathrm{d}S = 0 \tag{36}$$

contains contributions from the matrix boundaries S_1 and $S_2 \cup S^{\mathrm{p}}$, which vanish separately. The integral over the boundaries S_1 comprises two parts which cancel due to the applied periodic boundary conditions and the fact that the unit normals at $x_1 = \pm w$ point in opposite directions. The second contribution in (36) vanishes due to the boundary conditions (28).

The spatial discretization of Eq. (26) is done in the same manner as for Eq. (27), leading to

$$\mathbf{M}\dot{\boldsymbol{\rho}} = \mathbf{J}\boldsymbol{\kappa} - \mathbf{H}^*\boldsymbol{\kappa} + \mathbf{f}^*. \tag{37}$$

Here, the matrices $\mathbf{M}$ and $\mathbf{J}$ are identical to those in (33) and (34), respectively, and

$$\mathbf{H}^* = B^{-1}b^2 \int_{-w}^{w} \int_{-h}^{h} T\frac{\kappa}{\rho} \frac{\partial \mathbf{N}}{\partial x} \frac{\partial \mathbf{N}^\mathrm{T}}{\partial x} \, \mathrm{d}x_1 \, \mathrm{d}x_2 \tag{38}$$

is the diffusion matrix; the vector $\mathbf{f}^*$ contains the discretized source term (21) and contributions from the boundaries. The boundary terms vanish due to the same reasons discussed above for (36).

Integration of the integrals in (33)–(35) and (38) per triangular element is done by single-point integration with the integration point located at the center of each triangle. After assembling the contributions for Eqs. (37) and (32) from all elements, we obtain two independent sets of linear equations for the nodal values of the total and sign density rates $\dot{\boldsymbol{\rho}}$ and $\dot{\boldsymbol{\kappa}}$, respectively.

Thus, starting from a known stress configuration and dislocation density distribution, we can compute the elastic and plastic strain rates, as well as associated stress rates, and the rate of change of the dislocation density fields at a given instant t. To integrate the solution in time an adaptive time stepping procedure with a maximum allowable time step Δt_{crit} is adopted here. The critical time step Δt_{crit} is determined by the dislocation evolution subproblem and is defined as the minimum value of all element time steps Δt^{el} calculated from the stability condition

$$C_c^{\mathrm{el}} = \sqrt{\frac{1}{Pe^2} + \frac{1}{3}} - \frac{1}{Pe}, \tag{39}$$

where,

$$C_c^{\mathrm{el}} = \left| B^{-1}b\tau \frac{\Delta t^{\mathrm{el}}}{h^{\mathrm{el}}} \right|, \quad Pe = \left| \frac{\tau h^{el}}{2Tb\xi} \right|$$

are the element Courant and Peclet numbers, respectively, with h^{el} the element size; $\xi = \kappa/\rho$ for Eq. (26) and $\xi = 1$ for Eq. (27). Oscillations in the solution can be avoided when the element Peclet number $Pe \leqslant 1$ (Zienkiewicz and Taylor, 1991).

5. Summary of discrete dislocation results

In this section, we briefly summarize the results of discrete dislocations simulations of the problem at hand. The results to be presented are close to those obtained by Cleveringa et al. (1997, 1998, 1999a) but differ in the fact that here we do not assume an initial distribution of dislocation obstacles inside the matrix. There are no dislocations present initially, and dislocation sources are assumed to be distributed randomly in the matrix with a uniform density of $\rho_{\mathrm{n}} = 61.2L^{-2}$ for morphology (i) and $\rho_{\mathrm{n}} = 55.4L^{-2}$ for morphology (iii). The strength of the dislocation sources is chosen randomly from a Gaussian distribution with mean value $\bar{\tau}_{\mathrm{nuc}} = 1.9 \times 10^{-3}\mu$ and standard
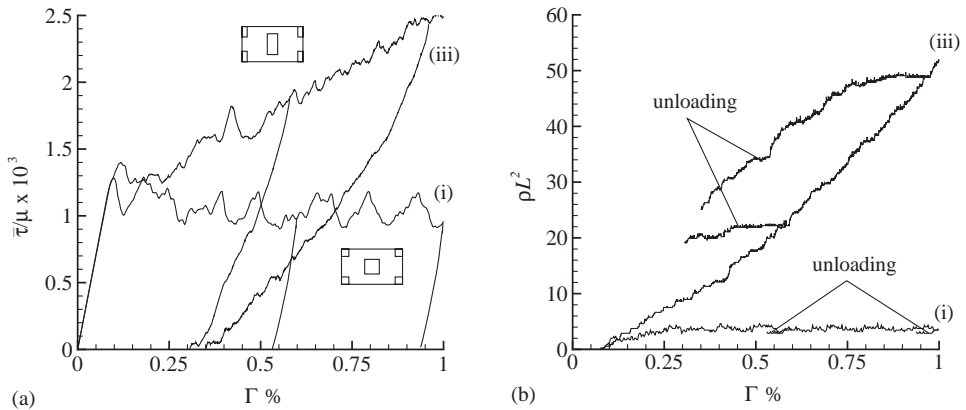
Fig. 2. Average shear stress $\bar{\tau}$ versus applied shear strain Γ for forward shearing and unloading from $\Gamma = 0.58\%$ and from $\Gamma = 0.96\%$ to $\bar{\tau} = 0$ for material (i) and material (iii) according to the discrete dislocation dynamics.

deviation $\Delta\tau_{\text{nuc}} = 0.2\bar{\tau}_{\text{nuc}}$. The nucleation time is taken to be $t_{\text{nuc}} = 2.6 \times 10^6 B/\mu$ for all sources.

Fig. 2a shows the overall stress response to shear for morphologies (i) and (iii). Even though there are no obstacles, the trends are equal to those found by Cleveringa et al. (1997, 1998). Morphology (i) gives rise to essentially perfect plasticity, with a small amount of softening upon overall yield, while morphology (iii) leads to almost linear hardening on average. The origin of this difference lies in the fact that there are unblocked channels of material for morphology (i) where unrestricted slip can take place; only a few dislocations that move over long distances are necessary to accommodate the applied shear, see Fig. 2b. A few slip planes that are blocked by one of the particles contain dislocations that are generated by virtue of the stress concentrations at the particle corners, see Fig. 3a. Not shown here is the observation, just like in (Cleveringa et al., 1997, 1998), that the response of material (i) is independent of the size of the particles.

The hardening found for morphology (iii) is caused by many dislocations piling up against the particles. This leads to polarized walls of dislocations on either side the central particle, corresponding to its rotation in the shearing direction. A number of these dislocations are geometrically necessary in the sense of Ashby (1970). Associated with this, the overall response is size dependent with smaller particles giving rise to a harder material (Cleveringa et al., 1998). Other characteristics are the development of several long pile ups against the corner particles (Fig. 3b) and the fact that the total dislocation density is much higher than for morphology (i), Fig. 2b. These characteristics translate into a deformation pattern as illustrated in Fig. 4.

Also shown in Fig. 2a is the response under unloading from pre-strains of $\Gamma = 0.58\%$ and 0.96%. In material (i) this occurs by elastic unloading without any significant change in the dislocation distribution. On the other hand, the long-range back stress developed in morphology (iii) gives rise to a very significant Bauschinger effect
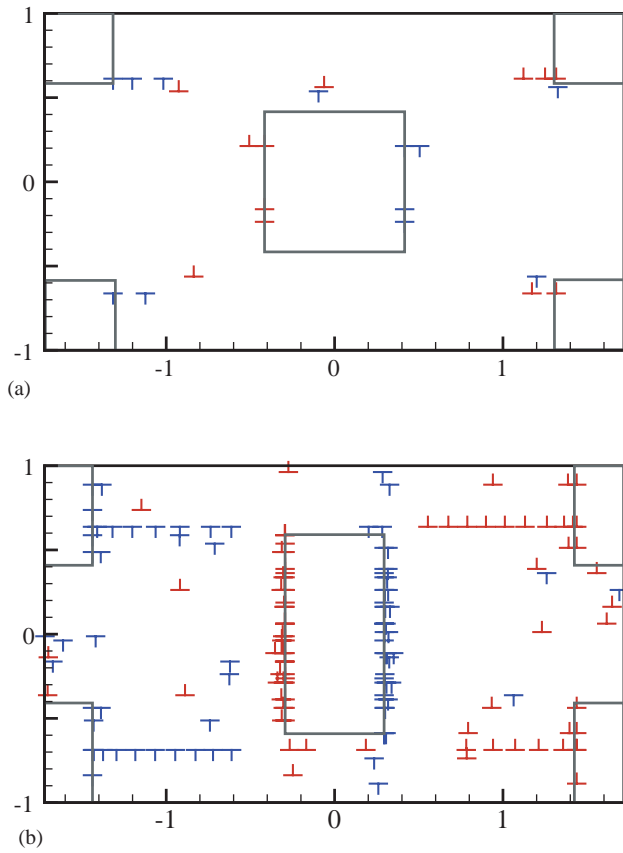
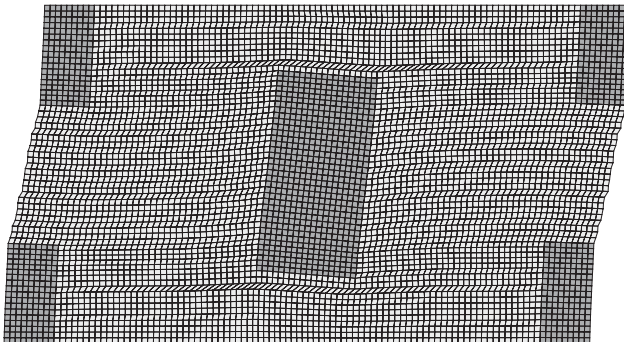Fig. 3. Dislocation distributions at $\Gamma = 0.6\%$ for (a) material (i) and (b) for material (iii).

Fig. 4. Deformed finite element mesh (displacements magnified by a factor of 20) showing the local distortions in material (iii) at the same instant, $\Gamma = 0.6\%$, as depicted in Fig. 3b.

associated with dissolution of the dislocation structure. This confirms the assertion of Cleveringa et al. (1999a) that hardening for this morphology originates predominantly from back stress.

6. Nonlocal crystal plasticity results

The discrete dislocation simulations discussed above will now be compared with the calculations based on the nonlocal continuum plasticity theory put forward in Sections 2 and 3. As in the discrete calculations, we start out from a stress free and dislocation free state, $\rho(\mathbf{r}, t_0) = \kappa(\mathbf{r}, t_0) = 0$. The results to be presented have been obtained using the same material parameters, whenever possible, as in the discrete dislocation calculations above, both for elastic and dislocation properties. The sources have the same densities as in the discrete dislocation simulations, but are distributed uniformly in the matrix. The strength of the dislocation sources per integration point is randomly chosen from the same Gaussian distribution as above. An almost uniform finite element mesh consisting of 102×60 quadrilateral elements is used.

It is important to note that, compared to the discrete dislocation simulations, the continuum theory has a few free parameters: the coefficient D in the back stress (13); the slip resistance τ_{res}, cf. (20); and the annihilation coefficient A. Their values do not follow from the derivation (although $D = 0.8$ has been suggested in (Groma et al., 2003)) and have to be specified additionally as material parameters. For comparison with the foregoing discrete dislocation results, the following parameter values have been employed: $A = 5$, $D = 1$ and $\tau_{\text{res}} = 15$ MPa.

6.1. Size effects

Fig. 5 shows the computed overall shear stress response to the prescribed shear Γ for the two morphologies (i) and (iii) for the reference cell size $h = L$. For comparison, the results of the discrete dislocation calculations from Section 5 are included. For morphology (iii) the result of the continuum calculations is also shown for the case of a uniform distribution of source strength ($\Delta\tau_n = 0$) with the reference value $\bar{\tau}_n = 1.9 \times 10^{-3}\mu$. Consistent with the discrete dislocation results, morphology (i) leads to a clear yield point with strain softening afterwards, while morphology (iii) exhibits nearly linear back stress hardening. The results for morphology (iii) for two different values of the $\Delta\tau_n$ show a strong dependence of the yield point on the strength distribution of the dislocation sources, but the average tangent modulus $d\bar{\tau}/d\Gamma$ is hardly affected by the source strength distribution.

The continuum dislocation distributions for the cases with $\Delta\tau_{\text{nuc}} = 0.2\bar{\tau}_{\text{nuc}}$ are shown in Figs. 6 and 7 in terms of the ρ and κ fields, respectively. The "noise" in the ρ-distributions in Fig. 6 for low values of ρ suggests that the chosen Galerkin-based method has some difficulties in obtaining stable solutions. Experiments with different meshes and time steps has convinced us nevertheless that the shown solution is sufficiently reliable for the present purpose. Qualitatively, the results in Figs. 6 and 7 show similar dislocation structures as found in the discrete dislocation analyses
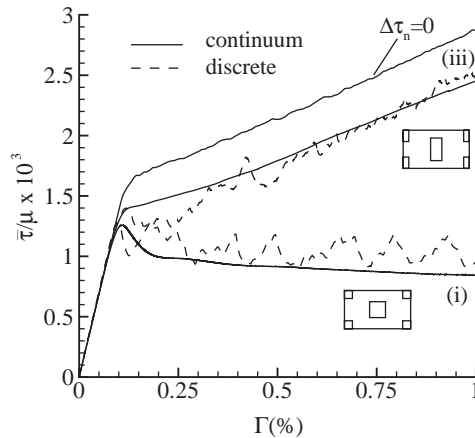
Fig. 5. Comparison of $\bar{\tau}$–Γ curves for material (i) and (iii) according to the discrete dislocation dynamics and the nonlocal continuum plasticity theory.

(Fig. 3): a few dislocations in the matrix, concentrated mostly in the unblocked channels for morphology (i), Fig. 6. Morphology (iii) gives strong piling up against the central reinforcing particle (Fig. 7a) with positive dislocations against the left-hand side and negative ones on the other side (Fig. 7b), associated with the rotation of the particle to accommodate the shear. As discussed in the previous section, morphology (iii) involves GNDs and the present continuum theory is able to predict them. Also seen in Fig. 7 are long pile-ups of the dislocations emanating from the corners of the particles; these too are consistent with the discrete dislocation findings by Cleveringa et al. (1997, 1998) and those shown in Fig. 3b.

 Contours of accumulated slip, γ, are shown in Fig. 8. The results in Fig. 8a for morphology (i) show that the applied macroscopic shear is accommodated in two coarse slip bands in the continuous unblocked channels of the matrix material, whereas in morphology (iii), Fig. 8b, a few bands of intense shearing near the top and bottom faces of the particles have developed. The latter reflect the rotation of the central reinforcing particle. It is interesting to note that the slip activity for morphology (i) is strongly controlled by the location of the weakest source; this explains why the slip distribution in Fig. 8a is not symmetric. This phenomenon is not seen in morphology (iii) since a large fraction of the dislocations are geometrically necessary. It is also of importance to note by comparison of Figs. 8b and 7b that the localization of deformation for morphology (iii) occurs in regions that are relatively dislocation free. Conversely, there is essentially no slip near the vertical sides of the central particle even though the dislocation density is high there. These observations are fully consistent with the results of discrete dislocation simulations, but notably different (Van der Giessen and Needleman, 2003) from the predictions of two other nonlocal continuum theories, due to Acharya and Bassani (2000) and Gurtin (2002) as presented in (Bassani et al., 2001) and (Bittencourt et al., 2003). In particular, the latter two theories predict high levels of slip near the vertical sides of the particle, just as predicted by
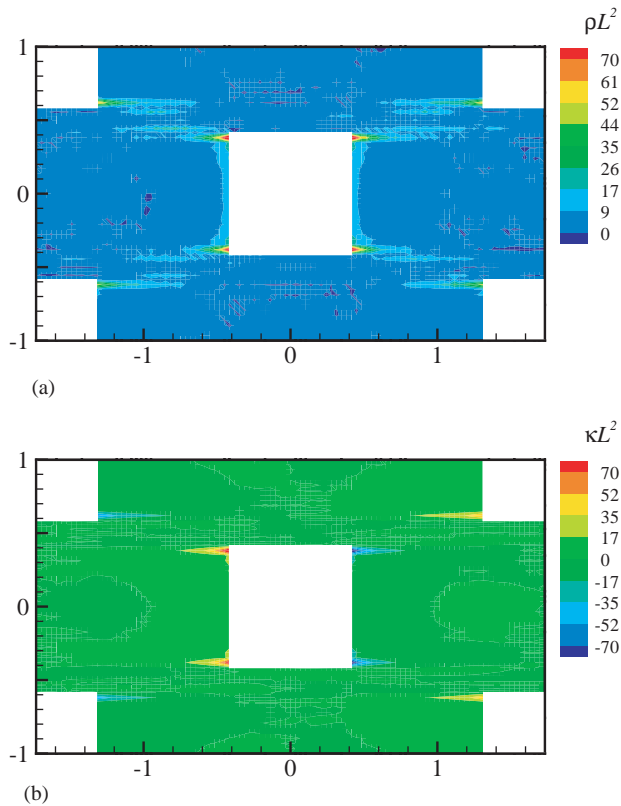
Fig. 6. Distribution of (a) the total dislocation density ρ and (b) the sign-dislocation density κ for material (i) at $\Gamma = 0.6\%$.

standard local continuum theory. The absence of this, just as in the discrete dislocation results of Fig. 4, is not merely due to the no-slip condition at these interfaces, because the same condition is used in the application of Gurtin's theory in (Bittencourt et al., 2003). Instead, it seems to originate from the fact that dislocation nucleation is not instantaneous and unlimited, as it is inherently assumed in standard phenomenological continuum theories as well as in the nonlocal version of Acharya and Bassani (2000) and Gurtin (2002).

The presence of GNDs in morphology (iii) but not in morphology (i) was used in Cleveringa et al. (1997, 1998) to substantiate the difference in hardening between the two materials, even though the area fractions of reinforcing phase are identical. The present continuum theory, using the same material constants, is able to distinguish between the different types of dislocation distributions but also the resulting difference in hardening.

A second consequence of the GNDs is that morphology (iii) shows a marked size dependence—with smaller being stronger—while morphology (i) is not. To assess the
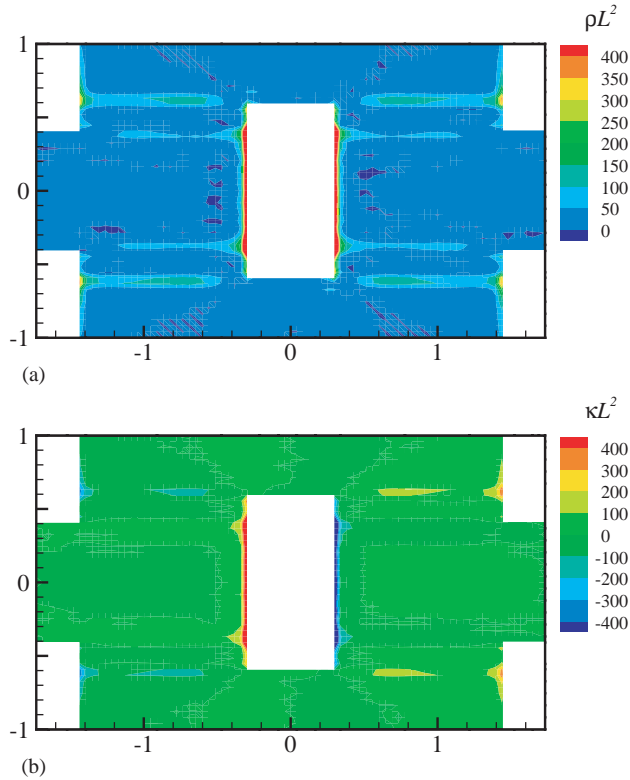
Fig. 7. Distribution of (a) the total dislocation density ρ and (b) the sign-dislocation density κ for material (iii) with $\Delta\tau_{\text{nuc}} = 0.2\bar{\tau}_{\text{nuc}}$ at $\Gamma = 0.6\%$.

ability of the present non-local continuum theory to recover these size effects, we have repeated the calculations but with smaller (so that $h = L/2$) and with larger ($h = 2L$) particles, but leaving the area fraction unchanged. Indeed, for morphology (i) the three responses are practically identical, while morphology (iii) exhibits the expected tendency, as shown in Fig. 9a. The figure displays the systematic trend that the hardening rate as well as the flow strength increase with decreasing particle size. The overall hardening for all sizes appears to be approximately linear with strain. Fig. 9b shows the evolution of the total dislocation density, normalized by the material length L, for morphology (iii). It is seen that the density of dislocations increases faster than linear with strain for all particle sizes. The dislocation density also increases with decreasing particle size, in agreement with the discrete dislocation results.

6.2. Unloading

The discrete dislocation results in Fig. 2a revealed a very distinct Bauschinger effect upon unloading for morphology (iii). This is largely due to the single slip configuration,
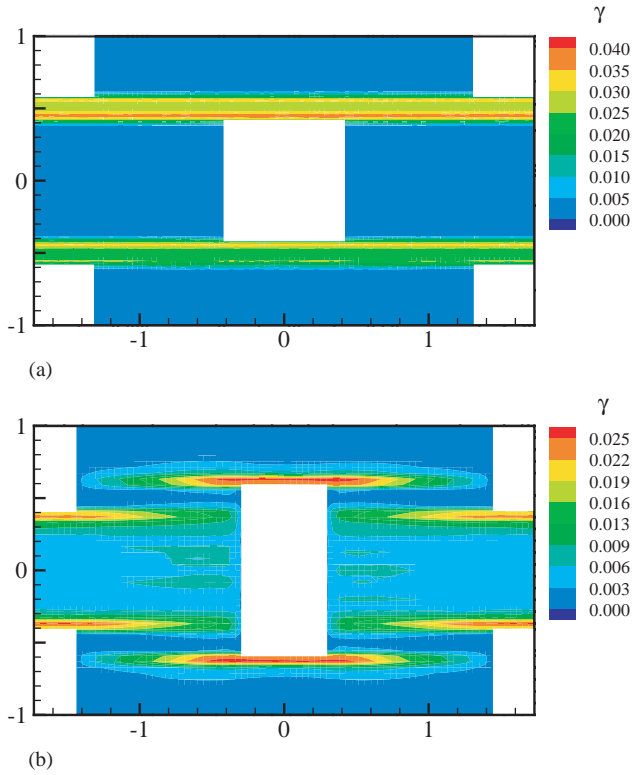
Fig. 8. Distribution of slip γ at $\Gamma = 0.6\%$ for (a) material (i) and (b) material (iii).
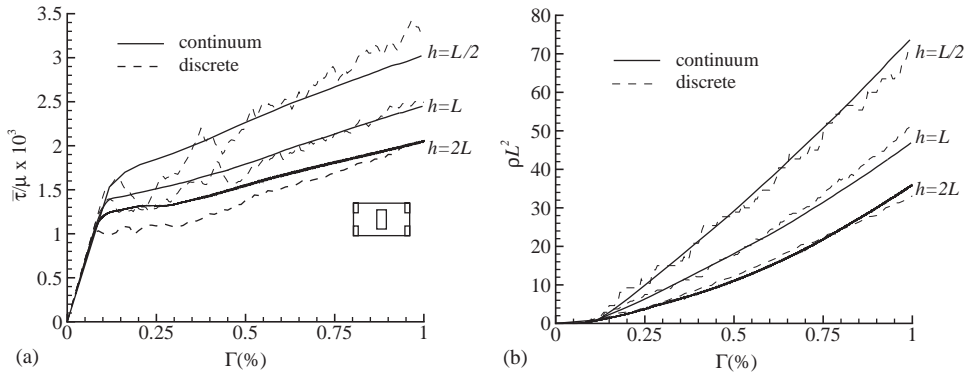

Fig. 9. Comparison of (a) stress–strain curve and (b) evolution of the total dislocation density ρ for material (iii) with three different particle sizes according to nonlocal continuum and discrete dislocation plasticity.
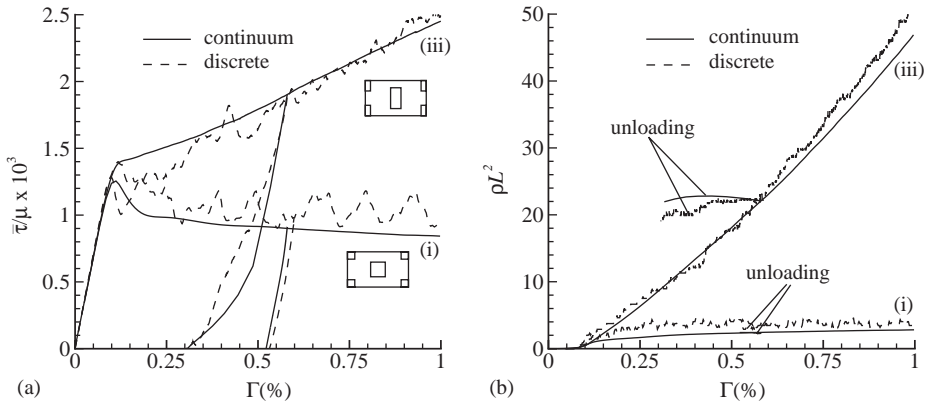
Fig. 10. Comparison of (a) stress–strain curve for forward shearing and unloading from $\Gamma = 0.58\%$, and (b) evolution of the total dislocation density ρ during forward loading and unloading for morphologies (i) and (iii) according to nonlocal continuum and discrete dislocation plasticity.

but is not present in standard local calculations (see Bittencourt et al., 2003). Also the nonlocal theory of Acharya–Bassani does not predict any Bauschinger effect (Bassani et al., 2001), but there is in Gurtin's theory (Bittencourt et al., 2003). To see the capabilities of the present theory, we have also carried out unloading computations using the continuum theory, from the same amounts of pre-strain as in Fig. 2a and at the same absolute value of the loading rate.

Fig. 10a shows a comparison of the average shear stress versus shear strain curves for both morphologies including unloading from $\Gamma = 0.58\%$ according to both calculations. Overall, the predictions of the nonlocal continuum plasticity are consistent with the findings of the discrete dislocation simulations. The two models predict an almost elastic response for morphology (i) and a strong Bauschinger effect for morphology (iii) with residual plastic strains of around 0.25%. However, there is some qualitative difference in the unloading response between the two models for morphology (iii). In case of the continuum theory, reverse plastic flow during unloading is delayed compared to the discrete dislocation results, even though the two models predict the same amount of residual strain. The evolution of the total dislocation density ρ during unloading, shown in Fig. 10b, reveals that the reverse plastic flow involves not only the motion of dislocations but also their annihilation, which is most clear for morphology (iii).

For morphology (iii), unloading from a pre-strain $\Gamma = 0.96\%$ is shown in Fig. 11. The onset of reverse plastic flow is more pronounced now than during unloading from a pre-strain $\Gamma = 0.58\%$, and also more pronounced than that predicted with discrete dislocations, Fig. 2a. Nevertheless, the predicted residual strain of around 0.35% agrees with the discrete dislocation results. It is important to note that the resulting residual strains in the continuum calculations depend on the chosen value of $\tau_{res} = 15$ MPa. To demonstrate this, an additional unloading calculation was carried out with $\tau_{res} = 20$ MPa instead of 15 MPa. An increase of the slip resistance decreases dislocation activity and
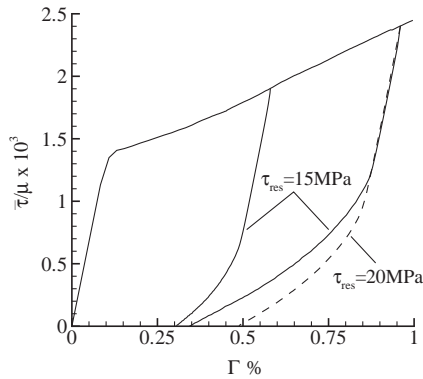
Fig. 11. Stress–strain curves for forward shearing and unloading from $\Gamma = 0.58\%$ and from $\Gamma = 0.96\%$ for material (iii) according to the nonlocal continuum theory. Unloading from $\Gamma = 0.96\%$ with $\tau_{res} = 20$ MPa instead of 15 MPa is shown for comparison.

leads to a less pronounced Bauschinger effect. Conversely, one can say that the value of τ_{res} can be fitted from unloading results.

7. Conclusion

We have formulated a non-local continuum crystal plasticity theory for single slip that involves standard continuum kinematics and two state variable fields: the dislocation density and the net-Burgers vector density. These densities are governed by two coupled evolution equations that describe their balance during drag-controlled dislocation glide, and which are derived from a statistical-mechanics treatment of an ensemble of gliding dislocations. The conservation law for the dislocation density is extended to account for dislocation generation from, for instance, Frank-Read sources and for annihilation. The non-locality of the theory is contained in the balance laws and the presence of a back stress that is controlled by the in-plane gradient of the net-Burgers vector density.

To investigate the capabilities of the theory, it has been applied to the problem of simple shearing of a model composite material, and compared to the discrete dislocation simulations by Cleveringa et al. (1997, 1998, 1999a). The continuum theory is shown capable of distinguishing between the responses of two different particle morphologies (with the same area fraction), one involving unblocked slip in veins of unreinforced matrix material, the other relying on particle rotations induced by plastic slip gradients and GNDs. The overall response as well as the local plastic deformation fields are in general accord with the discrete dislocation results. In addition, the size dependence of the behavior for the morphology that has GNDs is also picked up well.

The comparison has exemplified the importance of nucleation control: continuum theories have the inherent assumption that dislocations are present whenever and wherever they are needed. This is not physical. The present theory includes a model for

nucleation and does not make this assumption, which has a significant effect on the plastic flow field.

Calculation of the responses during forward shearing as well as unloading have clearly revealed that the theory involves two sources of hardening: (i) back stresses generated by long-range κ fields; (ii) slip resistance. The back stresses are related to gradients in κ, i.e. the density of GNDs, which in the present problem are associated with the rotation of the particles. Both hardening contributions enter the theory with a free coefficient, which needs to be fitted either to discrete dislocation simulations, as done here, or to experimental results. The slip resistance has been viewed here as a constant, but it can be extended to be a variable that evolves with deformation.

The theory belongs to the group of models like those of Aifantis (1984), Fleck and Hutchinson (1997), Shu and Fleck (1999) and Gurtin (2002) which involve additional boundary conditions compared to local continuum plasticity theories. Here, the additional boundary conditions enter through the density evolution equations. The model is distinctly different from Aifantis' (1984) proposition in that his theory does not incorporate the net-Burgers vector density; it differs from the latter three theories—Fleck and Hutchinson (1997), Shu and Fleck (1999) and Gurtin (2002)—in that they are entirely phenomenological while the present one has a solid dislocation basis. Accordingly, the additional boundary conditions have a clear physical meaning for the problem analyzed here: no dislocation motion at the interfaces with particles normal to the slip planes. Whether the model yields equally good agreement with discrete dislocation simulations for other boundary-value problems, just as bending (Cleveringa et al., 1999b) involving free surfaces, will be investigated in a subsequent paper.

Finally, it should be emphasized that the balance laws have been derived for single slip only. Obviously, for the theory to become versatile, it needs to be extended to multiple slip. The first steps into this direction have very recently been made by Zaiser et al. (2001).

Acknowledgements

References

Acharya, A., Bassani, J.L., 2000. Incompatibility and crystal plasticity. J. Mech. Phys. Solids 48, 1565–1595.

Aifantis, E.C., 1984. On the microstructural origin of certain inelastic models. J. Eng. Mater. Technol. 106, 326–330.

Asaro, R.J., 1983. Micromechanics of crystals and polycrystals. Adv. Appl. Mech. 23, 1–115.

Ashby, M.F., 1970. The deformation of plastically non-homogeneous materials. Phil. Mag. 21, 399.

Bassani, J.L., Needleman, A., Van der Giessen, E., 2001. Plastic flow in a composite: a comparison of nonlocal continuum and discrete dislocation predictions. Int. J. Solids Struct. 38, 833–853.

Bittencourt, E., Needleman, A., Gurtin, M.E., Van der Giessen, E., 2003. A comparison of nonlocal continuum and discrete dislocation plasticity predictions. J. Mech. Phys. Solids 51, 281–310.

Cleveringa, H.H.M., Van der Giessen, E., Needleman, A., 1997. Comparison of discrete dislocation and continuum plasticity predictions for a composite material. Acta Mater. 45, 3163–3179.

Cleveringa, H.H.M., Van der Giessen, E., Needleman, A., 1998. Discrete dislocation simulations and size dependent hardening in single slip. J. Physique IV 83–92.

Cleveringa, H.H.M., Van der Giessen, E., Needleman, A., 1999a. A discrete dislocation analysis of residual stresses in a composite material. Phil. Mag. A79, 863–920.

Cleveringa, H.H.M., Van der Giessen, E., Needleman, A., 1999b. A discrete dislocation analysis of bending. Int. J. Plasticity 15, 837–868.

Fleck, N.A., Hutchinson, J.W., 1997. Strain gradient plasticity. Adv. Appl. Mech. 33, 295–361.

Fleck, N.A., Muller, G.M., Ashby, F., Hutchinson, J.W., 1994. Strain gradient plasticity: theory and experiment. Acta Metall. Mater. 42, 475–487.

Groma, I., 1997. Link between the microscopic and mesoscopic length-scale description of the collective behaviour of dislocations. Phys. Rev. B 56, 5807–5813.

Groma, I., Balogh, P., 1999. Investigation of dislocation pattern formation in a two-dimensional self-consistent field approximation. Acta Mater. 47, 3647–3653.

Groma, I., Csikor, F., Zaiser, M., 2003. Spatial correlations and higher-order gradient terms in a continuum description of dislocation dynamics. Acta Mater. 51, 1271–1281.

Gurtin, M.E., 2000. On plasticity of crystals: free energy, microforces, plastic strain gradients. J. Mech. Phys. Solids 48, 989–1036.

Gurtin, M.E., 2002. A gradient theory of single-crystal viscoplasticity that accounts for geometrically necessary dislocations. J. Mech. Phys. Solids 50, 5–32.

Hirth, J.P., Lothe, J., 1968. Theory of Dislocations. McGraw-Hill, New York.

Kocks, U.F., Argon, A.S., Ashby, M.F., 1975. Thermodynamics and Kinetics of Slip. Prog. Mat. Sci. 19, 1–291.

Ma, Q., Clarke, D.R., 1995. Size dependent hardness of silver single crystals. J. Mater. Res. 10, 853–863.

Morton, K.W., 1996. Numerical solution of convection-diffusion problems. Chapman & Hall, London.

Shu, J.Y., Fleck, N.A., 1999. Strain gradient crystal plasticity: size-dependent deformation of bicrystals. J. Mech. Phys. Solids 47, 297–324.

Stölken, J.S., Evans, A.G., 1998. A microbend test method for measuring the plasticity length scale. Acta Mater. 46, 5109–5115.

Tabourot, L., Dumoulin, S., Balland, P., 2001. An attempt for a unified description from dislocation dynamics to metallic plastic behaviour. J. de Physique IV 11, Pr5/111–118.

Van der Giessen, E., Needleman, A., 1995. Discrete dislocation plasticity: a simple planar model. Model. Simul. Mater. Sci. Eng. 3, 689–735.

Van der Giessen, E., Needleman, A., 2003. GNDs in nonlocal plasticity theories: lessons from discrete dislocation simulations. Scr. Materialia 48, 127–132.

Zaiser, M., Carmen Miguel, M., Groma, I., 2001. Statistical dynamics of dislocation systems: the influence of dislocation–dislocation correlations. Phys. Rev. B 64, 224102–224111.

Zienkiewicz, O.C., Taylor, R.L., 1991. The finite element method, Fourth Edition. McGraw-Hill, New York.